LASER
& PHOTONICS
REVIEWS

Laser Photonics Rev. **9,** No. 5, 517–522 (2015) / **DOI** 10.1002/lpor.201500077

Abstract The unique electronic and mechanical properties, of graphene make it an ideal material for nanoelectromechanical system (NEMS) applications. Here, a miniature optical fiber current sensor based on a quasistatic graphene NEMS with a graphene membrane covering the hole on a pre-etched fiber tip and two gold electrodes on opposite sides of the tip has been demonstrated. The sensor overcomes the shortcomings of conventional optical fiber current sensors based on thermal effects, such as relatively low sensitivity, long response time, and huge device size; it has simultaneously a high sensitivity of 2.2 $\times$ 10^5 nm/A^2, a short response time of $\sim$0.25 s and a compact device size of $\sim$15 μm, and has found practical application. Using a smaller graphene membrane with better quality can reduce the response time to submillisecond levels with a more precise measurement system.

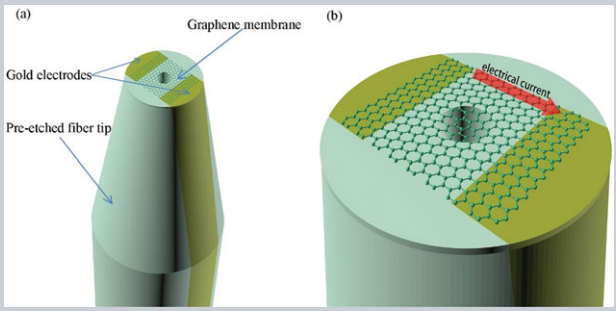

The sensor presented in this paper may pave the way for the practical usage of optical fiber current sensors based on thermal effects.

ORIGINAL PAPER

Miniature optical fiber current sensor based on a graphene membrane

Bi-Cai Zheng, Shao-Cheng Yan, Jin-Hui Chen, Guo-Xin Cui, Fei Xu*, and Yan-Qing Lu*

1. Introduction

Graphene is a single layer of carbon atoms that form a honeycomb lattice. It has drawn much attention in both scientific research and industrial application. Its remarkable electronic properties, such as ultrahigh electron mobility [1] and zero effective mass [2], make it a promising electronic material for the future. Graphene is also known as the strongest material ever measured, with a breaking strain of nearly 25% and a Young's modulus of 1 TPa [3]. Owing to its unique electronic and mechanical properties, graphene is an ideal material for use in nanoelectromechanical systems (NEMS). Accordingly, a variety of applications based on graphene NEMS have been developed, including force [4], mass [5], and pressure sensing [6]. NEMS are conventionally further classified into resonant and quasistatic NEMS [7], but most research attention has been focused on resonant graphene NEMS [8], leaving quasistatic graphene NEMS to be explored.

On the other hand, optical fiber current sensors have been widely used due to their ability to avoid electromagnetic interference [9]. One important method to realize optical fiber current sensors is to use magneto-optic effects, but sensors based on magnetic effects are normally large in size because of the relatively low Verdet constant [10]. Another method is to use thermal effects, such as the thermal-expansion effect or thermo-optic effect that is easier to be realized. Fiber Bragg gratings covered with conductive thin film [11, 12] and microfibers wrapped around a conductive rod [13–18] have been reported in recent years. However, the real applications are restricted by their large size, low precision, and, in particular, poor response time. The response time is limited by heat-generating and -transferring processes in what are commonly large heating elements, with typical values being seconds to minutes. In this paper, we report a miniature optical fiber current sensor based on a quasistatic graphene NEMS. With electrodes and a graphene membrane integrated on a pre-etched fiber tip, this sensor has a compact device size of $\sim$15 μm and a short response time of $\sim$0.25 s simultaneously; the response time can potentially be shortened to the order of submilliseconds if a smaller graphene membrane with better quality is used. An ultrahigh sensitivity of 2.2 $\times$ 10^5 nm/A^2, which is 3 orders of magnitude higher than previous reported results, is also realized, and the corresponding precision is 45.5 μA at 1 mA. Meanwhile, the thermal contraction behavior of a suspended graphene membrane is analyzed both theoretically and experimentally, and it will pave the way for potential applications of devices based on quasistatic graphene NEMS.

2. Fabrication

The sensor's configuration is shown in Fig. 1. The sensor was fabricated by etching a single-mode fiber with HF solution [19], depositing gold layers, and transferring a CVD-grown graphene membrane ($\sim$3 layers) [20].

National Laboratory of Solid State Microstructures, College of Engineering and Applied Sciences and Collaborative Innovation Center of Advanced Microstructures, Nanjing University, Nanjing 210093, P. R. China
*Corresponding author(s): e-mails: feixu@nju.edu.cn; yqlu@nju.edu.cn

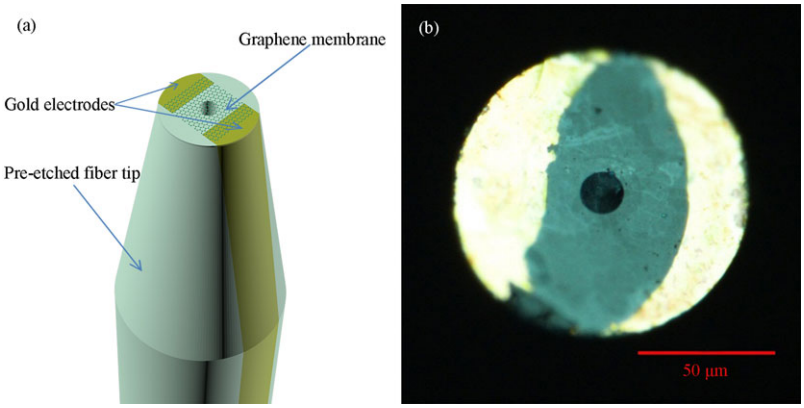

Figure 1 (a) Schematic of the sensor with a graphene membrane covering the hole and two gold electrodes on the pre-etched fiber tip. (b) A micrograph of the sensor. The diameter of the hole is 15.3 μm.

Fiber tip fabrication and functionalization: A single-mode fiber was cut and then immersed into an HF–water solution (~40%) for 9 min. Because of the different etching speeds of the core area and the cladding area [19], a hole in the center of the fiber tip was fabricated. The fiber tip was attached to a heating stage, whose temperature was set at 340 K, and a piece of paraffin was put onto the fiber without covering the tip. The paraffin melted and spread along the fiber to the tip's end. The spreading process was monitored by a microscope and the heating process paused as soon as the hole on the tip was covered by paraffin. A 100-nm thick gold layer was deposited on the area of the tip uncovered by paraffin and on the paraffin layer. The whole sample, together with the tip and paraffin, was then immersed in CCl_4 for 30 min to remove the paraffin and the part of the gold layer that was on the paraffin, leaving a gold electrode on the area of the tip uncovered by the paraffin. Another gold electrode was fabricated on the opposite side of the tip in the same way.

Graphene transfer: In this experiment, we used a commercial graphene membrane (~3 layers) that was grown on a copper foil by the chemical vapor deposition technique. The copper foil beneath the graphene was etched with a $FeCl_3$–water solution (1 mol/L), and the graphene membrane was transferred onto the surface of the deionized (DI) water in order to remove the residual Fe and Cu ions. The fiber tip, together with the hole and the electrodes on it, was attached to a high-precision translation stage with the fiber endface towards the floating graphene membrane. The fiber tip was lowered slowly, and the distance between the fiber tip and the floating graphene membrane was monitored by the reflection spectrum. Once the fiber tip touched the graphene membrane, it was pulled away from the DI water immediately, leaving the graphene membrane attached on the fiber endface. The sensor was then left to dry at room temperature in a cabinet for half an hour.

3. Optical characterization and current sensing

Optical characterization of the sensor in Fig. 2 was performed using an optical spectrum analyzer (OSA, YOKOGAWA AQ6370C) accompanied by an amplified spontaneous emission (ASE) source and a fiber-optic circulator. An electric current generated by an electric current source (KEITHLEY 2400 Source Meter) was coupled into the sensor using two contact pads, and the corresponding optical spectra were recorded by OSA when different currents were applied. The free spectrum range (FSR) of the sensor is 16 nm, and the corresponding cavity length can be calculated by $d = \lambda^2/(2\ \mathrm{FSR}) \approx 75\ \mu$m. The wavelength shift is 0.86 nm when the current is 2 mA, and the cavity length increases by ~42 nm accordingly, using $\Delta d = d\ \Delta\lambda/\lambda$ [20]. The reflectivity of two interfaces can be calculated to be 4.02×10^{-4} and 1.63×10^{-4} using the two-beam interference model. The relatively poor reflectivity and low Q-factor (~1220) of this grapheme-based F–P cavity are largely due to the imperfections induced in the device fabrication process, but they are still sufficient for the current-sensing application.

In order to investigate the current sensitivity of the sensor, the wavelength shift of the peak around 1550 nm was recorded when the current ascended from 0 mA to 2 mA and then descended from 2 mA to 0 mA. It can be seen in Fig. 3 that the wavelength of the resonant peak increases almost linearly with the square of current and that the corresponding current sensitivity is 2.2×10^5 nm/A^2, which is 3 orders of magnitude higher than the highest previously reported sensitivity of optical fiber current sensors [18]. The precision, δI, is defined as the minimum current vibration that can be detected by the OSA. It can be expressed as $\delta I = \delta\lambda/(d\lambda/dI) = \delta\lambda/(2I{\cdot}S)$, where $\delta\lambda$ is the wavelength resolution of OSA and S is the current sensitivity. Given $S = 2.2 \times 10^5$ nm/A^2 and $\delta\lambda = 0.02$ nm, the precision of the sensor is 45.5 μA at 1 mA. The sensitivity decreased a little when the current increased. This could be because of the temperature dependence of graphene's resistance [21], which was measured to decrease linearly with the increase of the current (from 1022 Ω to 942 Ω). A current larger than 2 mA was not applied to the sensor because of the possible damage it might cause. A larger layer number leads to the decrease of sheet resistance and less heat will be generated when applied with the same current, which results in a smaller sensitivity. However, a higher layer number can increase the contrast of the reflection spectrum in Fig. 2b because of the reflectivity dependence of graphene layers.

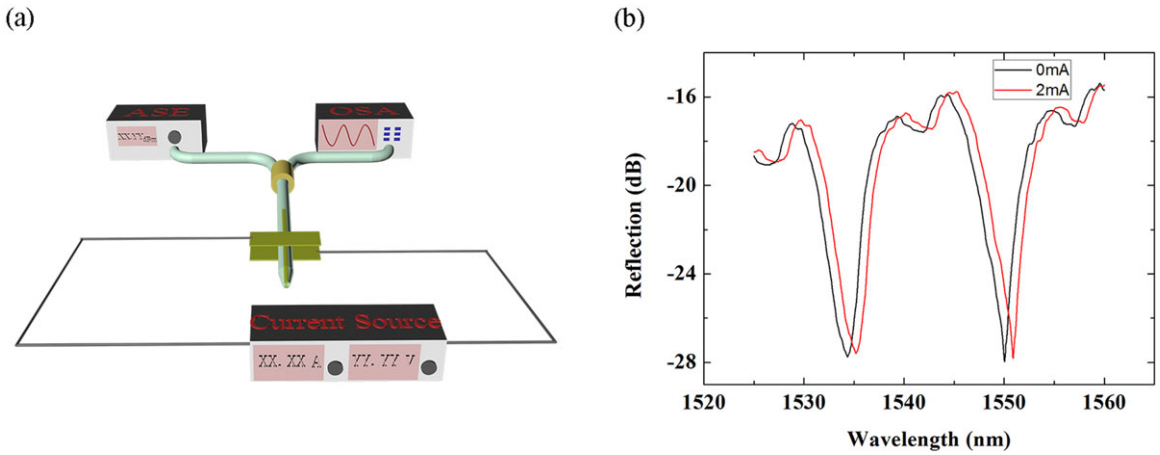

Figure 2 (a) Experimental setup. (b) Reflection spectra of the sensor when the current is 0 mA and 2 mA, respectively.

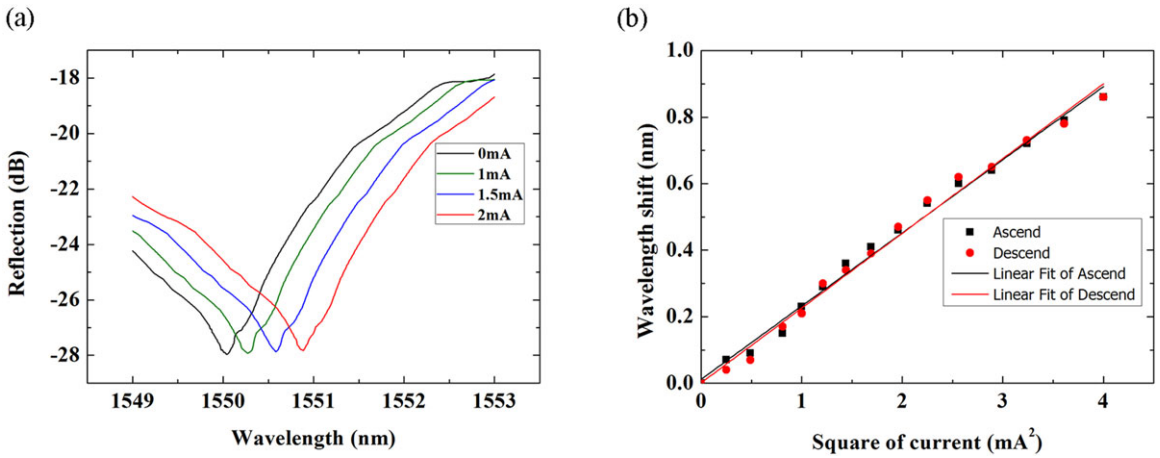

Figure 3 (a) Variation of reflection spectrum with the change of the current. The resonant wavelength shifted from 1550.04 nm to 1550.90 nm when the current was 0 mA, 1.0 mA, 1.5 mA, and 2.0 mA, respectively. (b) Wavelength shift as the function of the square of the current. The points are experimental values and the solid lines are linear fitting results. Both the ascending process and the descending process are presented.

The minimum limit of the current range, $I_{\min}$, can be calculated by using $I_{\min} = \sqrt{\delta\lambda/S}$. Due to the limitation of the wavelength resolution of OSA, the present $I_{\min}$ of our sensor is 0.3 mA, which can be improved by using a higher-resolution spectrometer to measure the wavelength shift. The measuring power variance of certain wavelengths is another possible method of improving this performance. The maximum limit of the current range, $I_{\max}$, is determined by two factors: the possible heat damage caused by defects and pollutants on the graphene membrane, and the nonlinear response of sensitivity caused by the temperature dependence of graphene's resistance. There are various ways to amplify $I_{\max}$, and adding a shunt resistor whose resistance is much smaller than the graphene membrane is probably the simplest way.

To further determine which effect caused the cavity length to increase, the sensor was put on a heating stage and the wavelength shifts were recorded at different temperatures. The measured temperature sensitivity of the sensor is 9.4 pm/K, which means that when the temperature increased by 91.5 K, the cavity length increased by ∼42 nm. According to the ideal gas equation, the air pressure in the hole would rise considerably with the temperature change if the graphene membrane were perfectly impermeable, and the cavity length change would be much larger than 42 nm [20]. As a result, the graphene membrane was inferred to be permeable to air, which could possibly be because of small leaking spots induced in the transferring process, and so the thermal-expansion effect of air should not be taken into consideration. On the other hand, the calculated cavity length change (∼3 nm) caused by the thermal expansion effect of fiber [22] is 1–2 orders of magnitude smaller than the experimental result.

After neglecting the thermal expansion effects of fiber and air, the negative thermal expansion effect of graphene (coefficient: $\alpha = -8 \times 10^{-6}$ K^{-1}) is the only possible explanation for this phenomenon [23, 24]. Meanwhile, the temperature at a certain wavelength shift in Fig. 4 can be

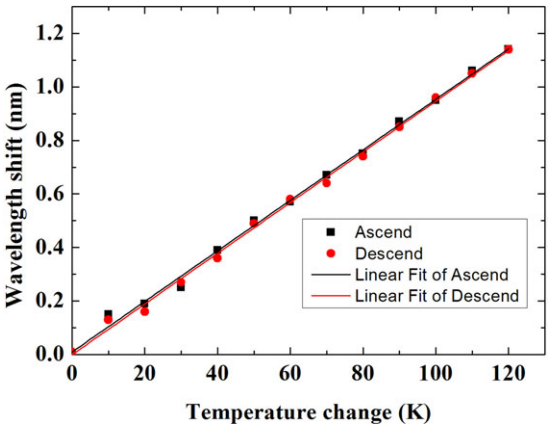

Figure 4 Wavelength shift as a function of temperature change. The points are experimental values and the solid lines are linear fitting results. Both the ascending process and the descending process are presented.

treated as the temperature of graphene at the same wavelength shift when the sensor is heated by the current. Thus, it can be inferred that when the sensor is heated by the current, the temperature change of graphene has a linear relationship with the square of current and the corresponding equation is $\Delta T = \gamma I^2$, where γ is a constant associated with the device configuration. In order to simulate the thermal contraction behavior, the graphene membrane is assumed to be sunken towards the hole on the tip after the transferring process. For simplicity, the shape of it is modeled as the equation below [25]:

$$z(r, \phi) = -D(r - R)^2(r + R)^2 / R^4,$$

where D is the deflection at the center of the graphene membrane and R is the radius of the graphene membrane. Due to the negative thermal expansion coefficient, the graphene membrane will contract uniformly with the rise in temperature, leading the coefficient D to decrease and the cavity length to increase. This phenomenon is illustrated in Fig. 5.

In Fig. 5b, the "temperature change" axis can be replaced by "square of current" using the previously proved equation of $\Delta T = \gamma I^2$. The "cavity length change" axis can also be replaced by "wavelength shift" using the equation of $\Delta d = d\ \Delta\lambda/\lambda$. After this transformation of horizontal and vertical axes, we find that the simulated results in Fig. 5b fit very well with the experimental data in Fig. 3b.

4. Response time

One key parameter for an electric current sensor is its response time, which is defined as the time to go from 10% to 90% of the difference between the lowest power and the highest power and vice versa [26]. For conventional optical fiber current sensors based on thermal effects, a relatively long response time is the major technological challenge that limits their applications. The main reason for this is that heat-generating elements (conductive thin films and metal rods) and heat-sensitive photonic elements (microfibers and fiber Bragg gratings) are commonly separate devices in previous sensors. For our sensor, the suspended graphene membrane acts as the heat-generating element and heat-sensitive photonic element at the same time, allowing the sensor to take less time to stabilize. Meanwhile, our sensor is a very compact one among all fiber current sensors based on thermal effects, which is also favorable for fast response speed.

In order to measure the response time of the sensor, the ASE and OSA were replaced by a tunable laser (AGILENT 8163B, 1547 nm, 10 mW) and a power meter (THORLABS PM100D, sampling frequency: 10 Hz), respectively. The electric current source with 2 mA output was switched on and then switched off within 10 s. The corresponding optical power data were recorded by the power meter and are shown in Fig. 6. It can be inferred that the response time of the sensor is 0.25 ± 0.05 s, which is one order of

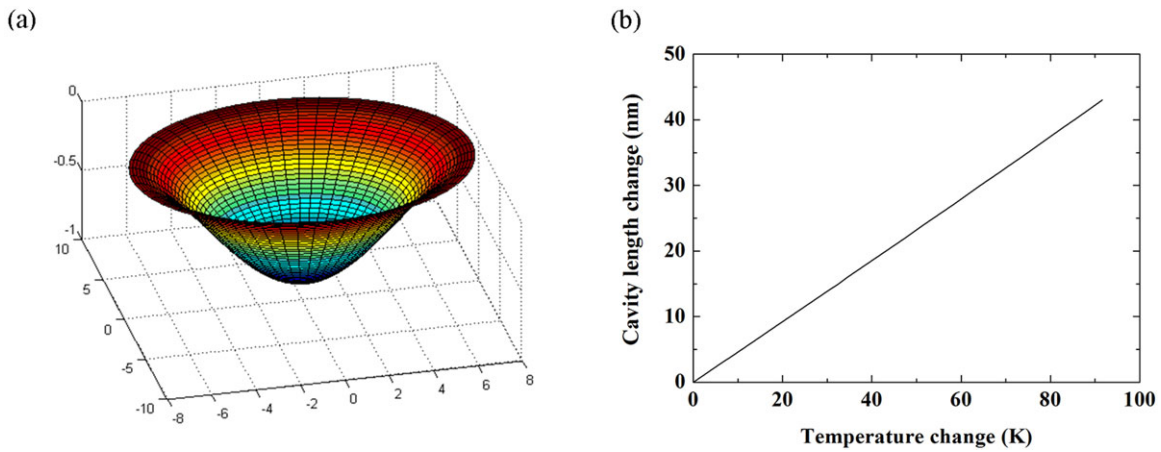

Figure 5 (a) A simplified model of the sunken graphene membrane. D is set at 854 nm in order to fit the experimental data. The unit in this figure is μm. (b) Simulated temperature response of the cavity length.

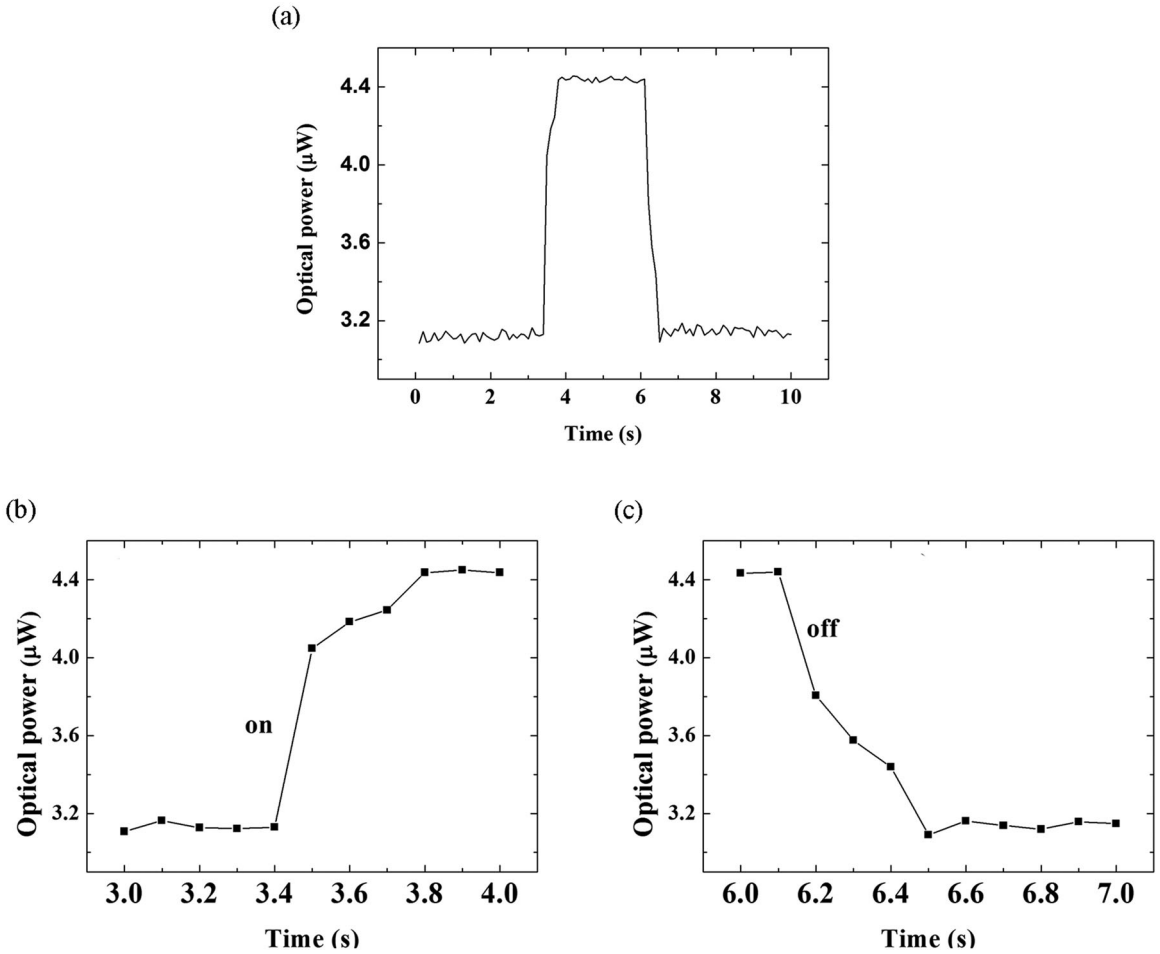

Figure 6 (a) Optical power data within 10 s. (b), (c) Enlarged portions of (a). The current source was turned on at 3.4–3.5 s and then turned off at 6.1–6.2 s. It took 0.3–0.4 s for the sensor to stabilize. The corresponding response time is around 0.25 s.

magnitude faster than previous optical fiber current sensors based on thermal effects [14, 15].

The response time is concerned with three major factors, which are heat generation, heat stabilization and mechanical response. Heat generation is an intrinsically fast physical phenomenon and its time can be neglected. Considering that the area effectively affected by the heat is tens of micrometers in diameter at most, the heat stabilization time is roughly calculated to be $\sim 10^{-4}$ s. The mechanical response time is at least at the submicrosecond level because resonant graphene NEMS devices with the same diameter can operate at MHz [4]. Therefore, we can reasonably estimate that the response time can reach submillisecond levels.

Our experimental result is severely restricted by the sampling frequency of the optical power meter that is only 10 Hz. Meanwhile, low-quality graphene with defects and contaminants requires the sensor to take more time to stabilize. The corresponding solutions are to use a more precise measuring system and high-quality graphene. Moreover, reducing the membrane's size is favorable for the response time because less graphene needs to be heated.

5. Conclusions and outlook

In conclusion, an optical fiber current sensor based on thermally actuated quasistatic graphene NEMS is experimentally demonstrated, and the sensor has a high sensitivity of 2.2×10^5 nm/A^2, a short response time of $\sim$0.25 s and a compact device size of $\sim 15\ \mu$m. The functional element is a sunken graphene membrane, whose shape changes with the variation of temperature due to the negative thermal expansion effect of graphene. The response time of the sensor can be more accurately measured if a frequency-tunable pulsed current source, an ultrafast photodetector, and an oscilloscope are used. The response time can also be potentially shortened to submillisecond levels with a more compact device size and a better graphene membrane, which can be realized by etching a tapered fiber with shorter time and using a mechanically exfoliated graphene sheet, respectively. When it comes to practical applications, other temperature sensitive devices, such as fiber Bragg gratings and inline F–P microcavities, can be integrated with the sensor in order to compensate for the temperature variance of the surrounding environment. Also, the sensor can be sealed into a

capillary to make it more robust while remaining compact. The unique device configuration demonstrated in this paper may find other sensing applications, such as magnetic field sensing based on the Lorentz force and electric field sensing based on the electrostatic force.

Acknowledgments. This work is supported by the National 973 program under contract No. 2012CB921803 and 2011CBA00205, the National Science Fund for Excellent Young Scientists Fund (61322503), the National Science Fund for Distinguished Young Scholars (61225026) and the National Natural Science Foundation of China (61475069).

Received: 26 March 2015, **Revised:** 2 July 2015,
Accepted: 22 July 2015

Published online: 13 August 2015

Key words: optical fiber, current sensor, quasistatic graphene NEMS, negative thermal expansion effect.

References

[1] K. I. Bolotin, K. Sikes, Z. Jiang, M. Klima, G. Fudenberg, J. Hone, P. Kim, and H. Stormer, Solid State Commun. **146**, 351 (2008).
[2] A. C. Neto, F. Guinea, N. Peres, K. S. Novoselov, and A. K. Geim, Rev. Mod. Phys. **81**, 109 (2009).
[3] C. Lee, X. Wei, J. W. Kysar, and J. Hone, Science **321**, 385 (2008).
[4] R. A. Barton, B. Ilic, A. M. van der Zande, W. S. Whitney, P. L. McEuen, J. M. Parpia, and H. G. Craighead, Nano Lett. **11**, 1232 (2011).
[5] C. Chen, S. Rosenblatt, K. I. Bolotin, W. Kalb, P. Kim, I. Kymissis, H. L. Stormer, T. F. Heinz, and J. Hone, Nature Nanotechnol. **4**, 861 (2009).
[6] J. S. Bunch, S. S. Verbridge, J. S. Alden, A. M. van der Zande, J. M. Parpia, H. G. Craighead, and P. L. McEuen, Nano Lett. **8**, 2458 (2008).
[7] K. Ekinci and M. Roukes, Rev. Sci. Instrum. **76**, 061101 (2005).
[8] R. A. Barton, J. Parpia, and H. G. Craighead, J. Vac. Sci. Technol. B **29**, 050801 (2011).
[9] W.-W. Lin, Opt. Eng. **42**, 896 (2003).
[10] Y. Ning, Z. Wang, A. Palmer, K. T. Grattan, and D. A. Jackson, Rev. Sci. Instrum. **66**, 3097 (1995).
[11] D. Jia, L. Zhao, and Y. Lin, in Photonics Asia 2004 (International Society for Optics and Photonics, 2005), pp. 515.
[12] S. Yang, H. Meng, X. Dong, Y. Xiang, and X. Dong, in International Symposium on Optoelectonics and Microelectronics (International Society for Optics and Photonics, 2001), pp. 219.
[13] X. Guo, Y. Li, X. Jiang, and L. Tong, Appl. Phys. Lett. **91**, 073512 (2007).
[14] K. Lim, S. Harun, S. Damanhuri, A. Jasim, C. Tio, and H. Ahmad, Sens. Actuators A: Phys. **167**, 60 (2011).
[15] A. Sulaiman, S. Harun, I. Aryanfar, and H. Ahmad, Electron. Lett. **48**, 943 (2012).
[16] A. Sulaiman, S. W. Harun, F. Ahmad, S. F. Norizan, and H. Ahmad, IEEE J. Quantum Electron. **48**, 443 (2012).
[17] G. Chen, G. Brambilla, and T. Newson, Electron. Lett. **49**, 46 (2013).
[18] X. Xie, J. Li, L.-P. Sun, X. Shen, L. Jin, and B.-O. Guan, Sensors **14**, 8423 (2014).
[19] M. S. Kaltenbach, A. S. Barber, G. V. Diaz, and M. A. Arnold, Anal. Lett. **24**, 2123 (1991).
[20] J. Ma, W. Jin, H. L. Ho, and J. Y. Dai, Opt. Lett. **37**, 2493 (2012).
[21] Q. Shao, G. Liu, D. Teweldebrhan, and A. Balandin, Appl. Phys. Lett. **92**, 202108 (2008).
[22] J.-L. Kou, S.-J. Qiu, F. Xu, and Y.-Q. Lu, Opt. Exp. **19**, 18452 (2011).
[23] D. Yoon, Y.-W. Son, and H. Cheong, Nano Lett. **11**, 3227 (2011).
[24] V. Singh, S. Sengupta, H. S. Solanki, R. Dhall, A. Allain, S. Dhara, P. Pant, and M. M. Deshmukh, Nanotechnology **21**, 165204 (2010).
[25] B.-C. Zheng, W. Luo, F. Xu, and Y.-Q. Lu, Phys. Rev. A **89**, 043810 (2014).
[26] S. Borini, R. White, D. Wei, M. Astley, S. Haque, E. Spigone, N. Harris, J. Kivioja, and T. Ryhänen, ACS Nano **7**, 11166 (2013).